A GEOCHEMICAL STUDY OF RHYOLITIC MELT INCLUSIONS IN IGNEOUS PHENOCRYSTS FROM LOWER DEVONIAN BENTONITES

by

Benjamin Hanson

A Dissertation

Submitted to the University at Albany, State University of New York

in Partial Fulfillment of

the Requirements for the Degree of

Doctor of Philosophy

College of Arts and Sciences

Department of Geological Sciences

1995

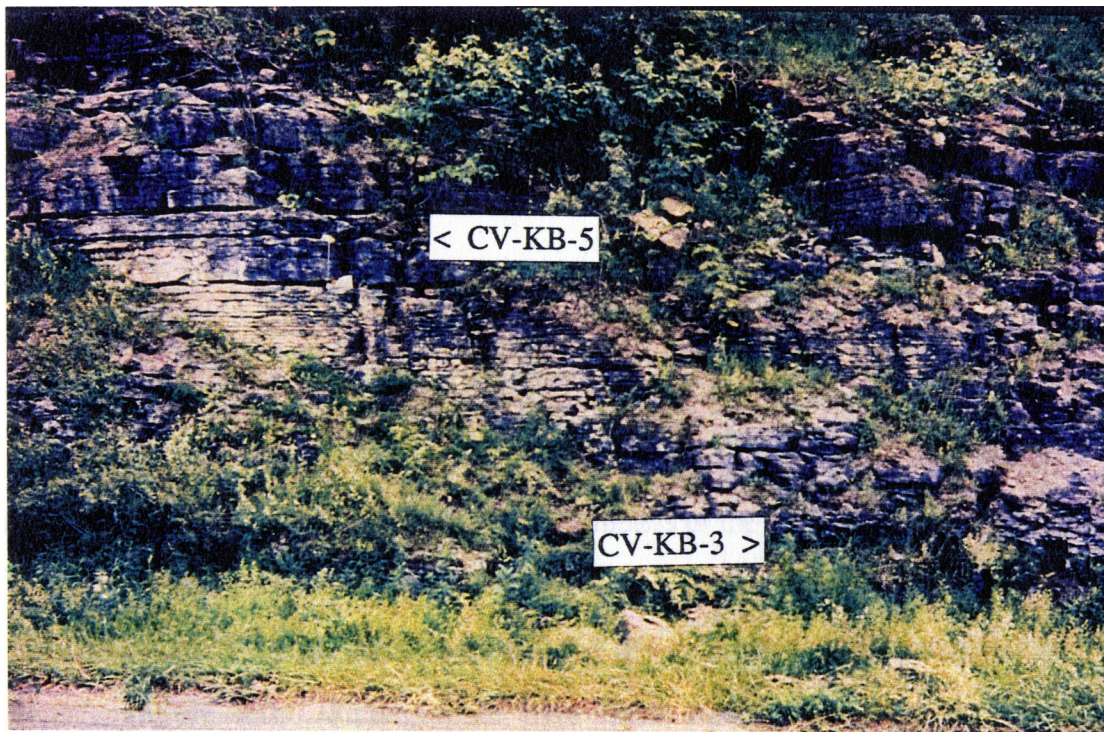

Figure 2.3. Photograph of the Kalkberg Formation on the south side of US Route 20, approximately 10 meters east of the abandoned railroad overpass at the Cherry Valley locality (locality #1). Arrows show the locations of bentonites CV-KB-3 and CV-KB-5.

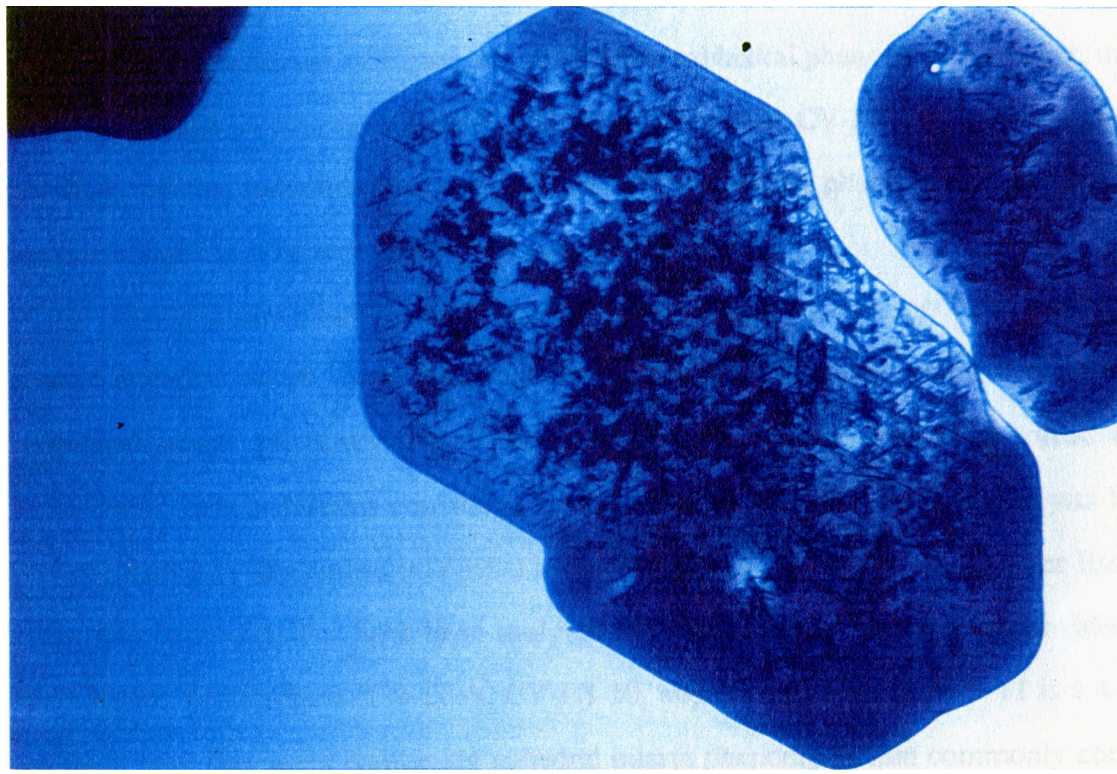

Figure 2.5. Transmitted light photomicrograph (in plane polarized light) of biotite flakes from CV-KB-3. The black inclusions are rutile crystals. Field width of photomicrograph is approximately 300 μm.

Figure 2.6. Photograph of the Kalkberg Formation on the south side of US Route 20, approximately 0.5 km west of State Road 10, at the Sharon Springs locality (locality #2). Arrows show the locations of bentonites SHS-KB-2 and SHS-KB-4.

Figure 2.8. Photograph of the upper Kalkberg and New Scotland Formations that outcrop on the south side of US Route 88, approximately 1.1 km from the Cobleskill exit (locality #3). Arrows show the positions of COB-NS-6 and COB-NS-8.

Figure 2.9. Photograph of the upper Oriskany and Esopus Formations that outcrop on the south side of US Route 88, approximately 0.5 km from the Cobleskill exit (locality #3). The contact between the Oriskany (DO) and Esopus (DE) Formations is shown.

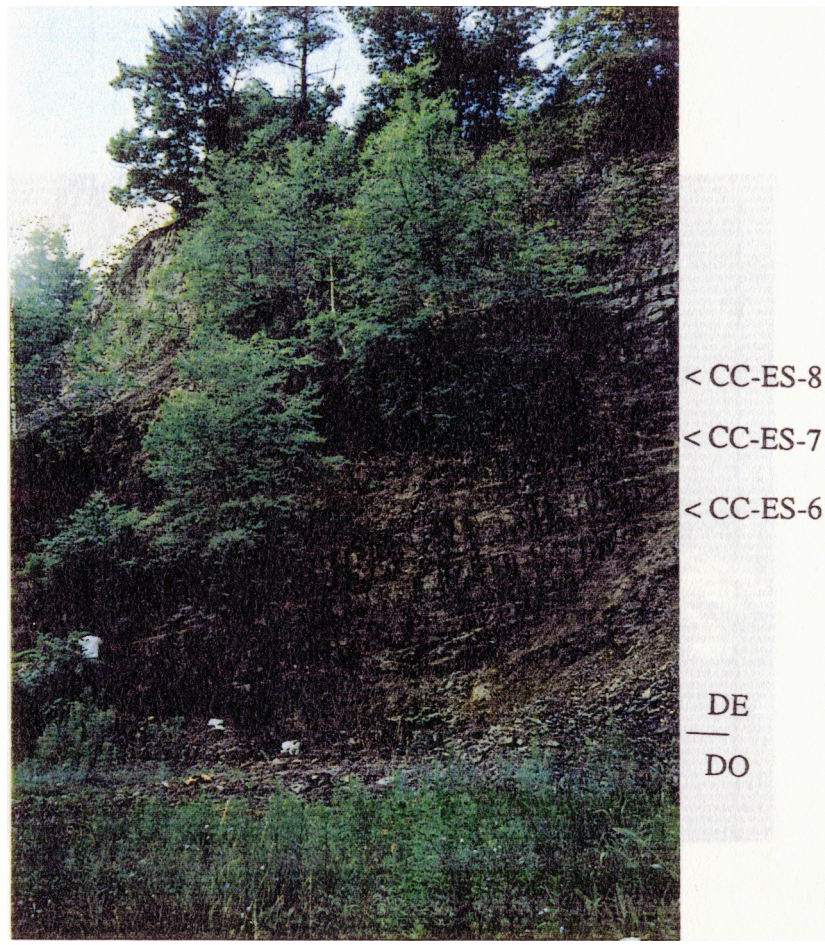

Figure 2.11. Photograph of the lower member of the Esopus Formation on the west side of County Road 102, to the south of Callanans Corners, NY (locality #5). Arrows show the stratigraphic positions of selected bentonites and the contact between the Oriskany (DO) and the Esopus (DE) is indicated. Person wearing white shirt is visible on the left edge of the photo sampling CC-ES-6. Photo by W. Kidd.

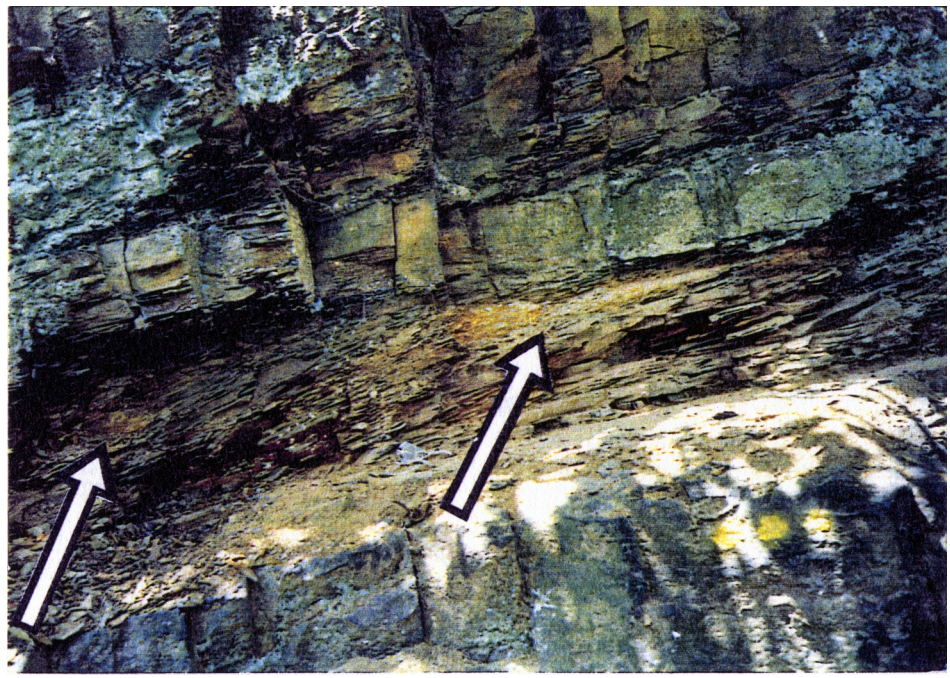

Figure 2.12. Photograph of bentonite CC-ES-6, which occurs in discrete "pods" at the top of the shaley interval (arrows indicate bentonite pods). The bentonite is tan at the edges of the pods and is gray in the middle. The shaley layers between the massive, cherty layers display a distinct cleavage at an angle to bedding. Note the hand lens for scale. Photo by W. Kidd.

Figure 2.15. Photograph of the New Scotland formation at Broncks Lake, NY (locality #7). Arrows show the position of the two bentonites containing melt-inclusion-bearing quartz phenocrysts at this outcrop. Person for scale is shown on the roadside.

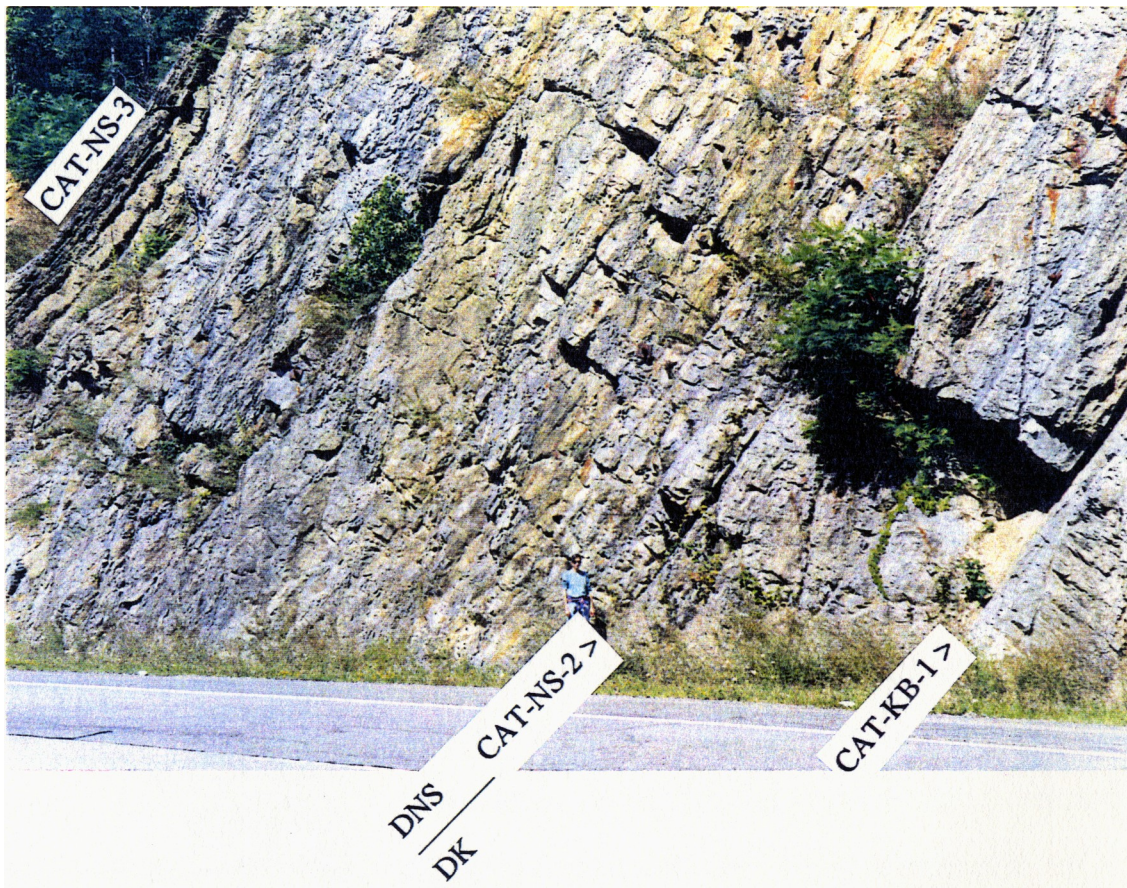

Figure 2.17. Photograph of the New Scotland Formation on the north side of State Route 23, at Catskill, NY (locality #8). Arrows show position of sampled bentonites and the boundary between the Kalkberg (DK) and the New Scotland (DNS) Formations is shown. Person is shown on the roadside for scale.

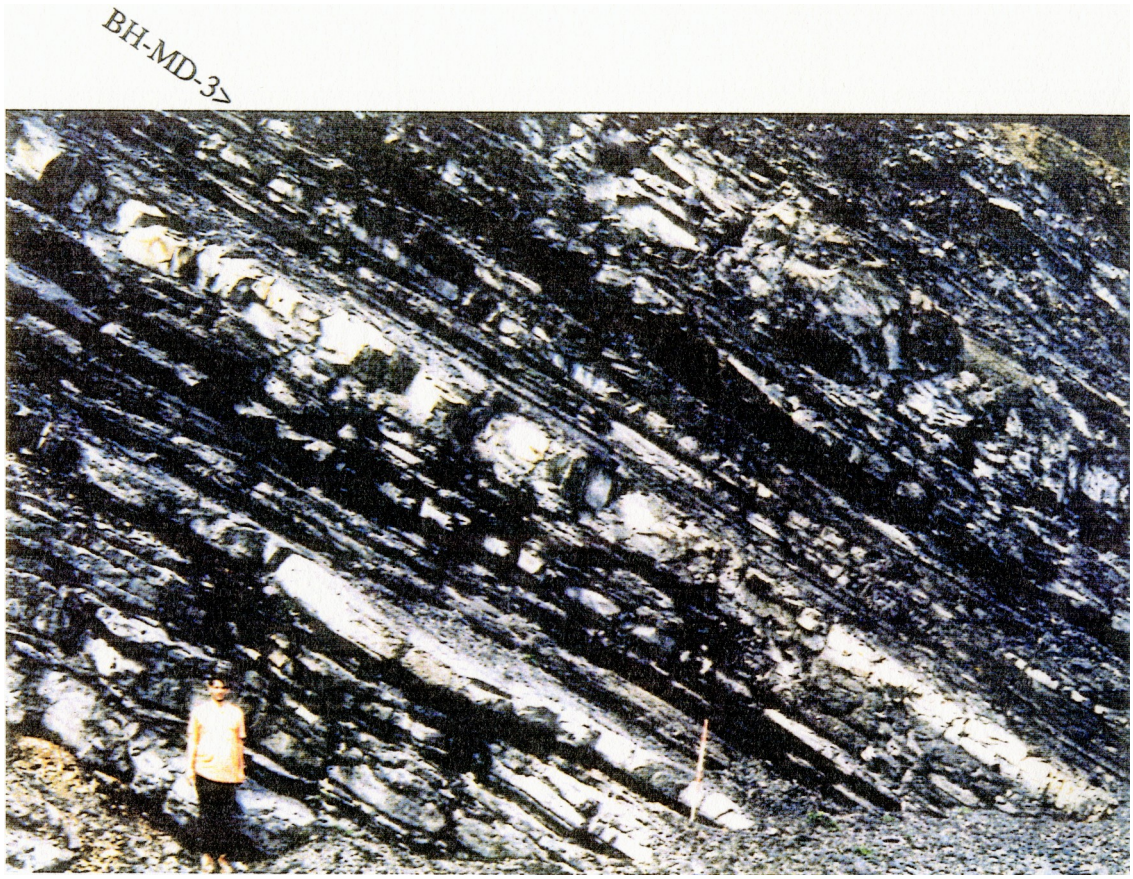

Figure 2.21. Photograph of the upper Corriganville Formation and the lower Mandata Formation on the north side of US Route 22, at Bald Hill, PA (locality #11). Arrows show the stratigraphic position of BH-MD-3 and the contact between the Corriganville (DC) and Mandata (DM) Formations. Right side of photograph is in a stratigraphically higher position.

Figure 2.23. Photograph of the Upper Keyser, Corriganville, and lower Mandata Formations on the west side of US Route 220, at Cessna, PA (locality 12). The New Creek-Corriganville Formation boundary is to the left of the red car. The left side of photograph is in a higher stratigraphic position.

Figure 2.25. Photograph of the upper Keyser, Corriganville and Lower Mandata Formations on the north side of the abandoned railroad cut at Corriganville, MD (locality #14). Arrows show the formation boundaries and the stratigraphic position of COR-MD-1. Right side of photograph is in a stratigraphically higher position.

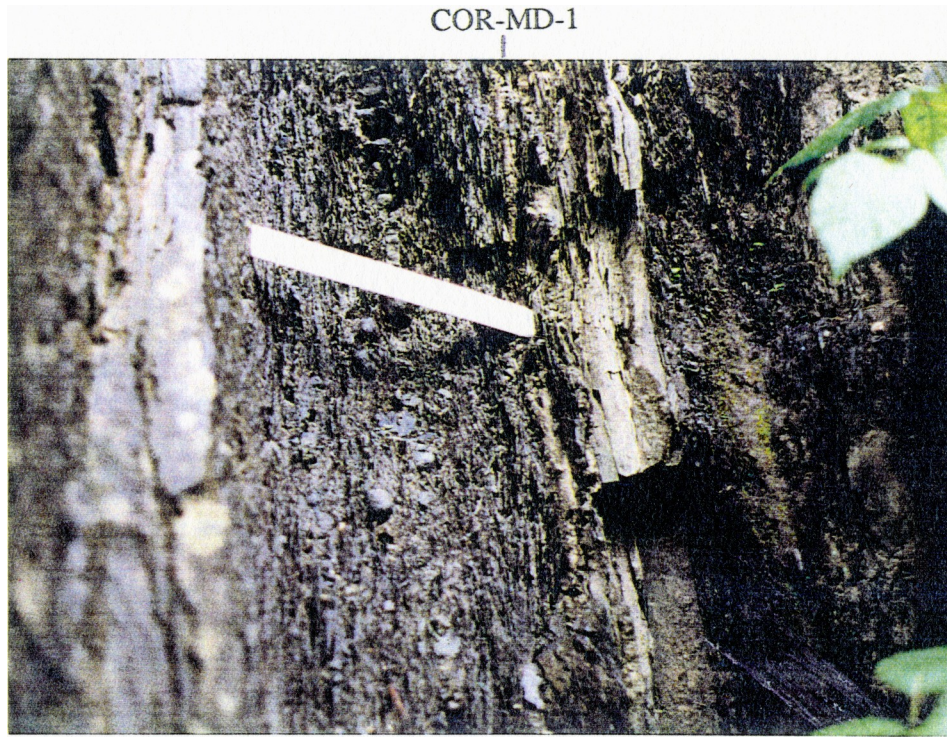

Figure 2.26. Photograph of the stratigraphic position of bentonite (thin tan layer at the right side of the 12 inch ruler) COR-MD-1 relative to the phosphate nodule zone (see text and Figure 2.27). Right side of photograph is in a stratigraphically higher position.

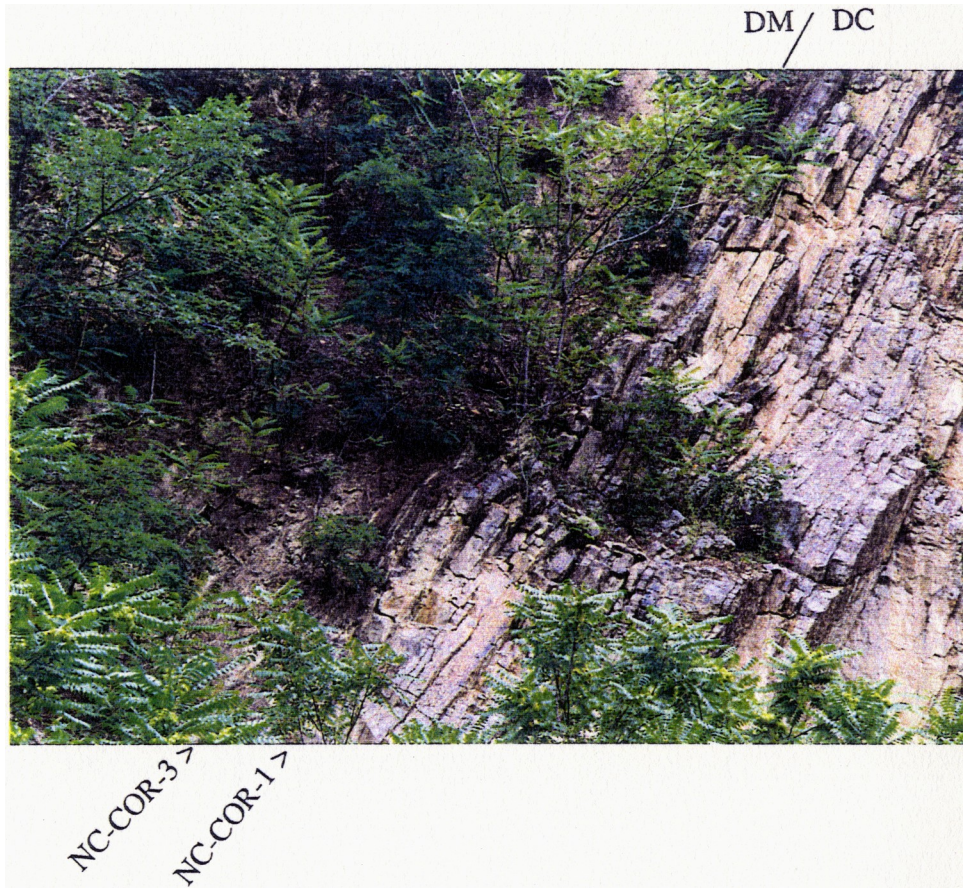

Figure 2.28. Photograph of the west side of an abandoned quarry at the intersection of US Route 50 and State Road 927, in New Creek, WV (locality #15). The arrows show the positions of the bentonites that contain melt-inclusion-bearing quartz phenocrysts within the section and the contact between the Corriganville (DC) and the Mandata (DM) Formations is indicated. Left side of photograph is in a stratigraphically higher position.

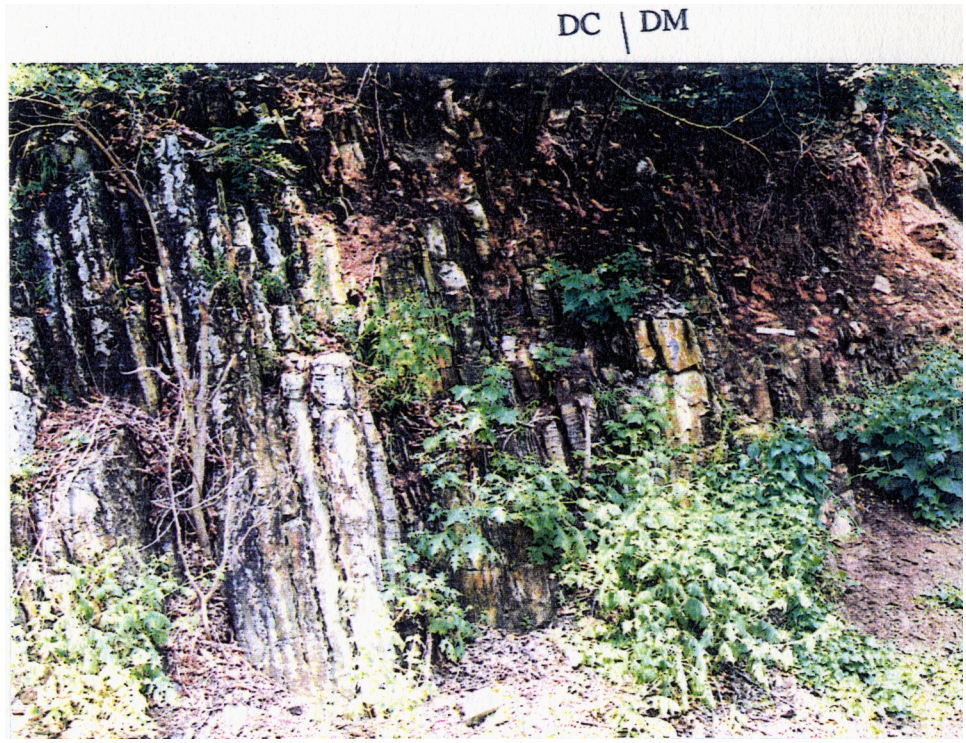

Figure 2.30. Photograph of the Upper Keyser, Corriganville, and lower Mandata Formations on the north side of the access road to the Smoke Hole National Recreation Area, WV (locality #16). The contact between the Corriganville (DC) and Mandata (DM) Formations is shown. The right side of the ruler (1 foot) at the right side of the photograph is on SMH-MD-3. Right side of the photograph is in a stratigraphically higher position.

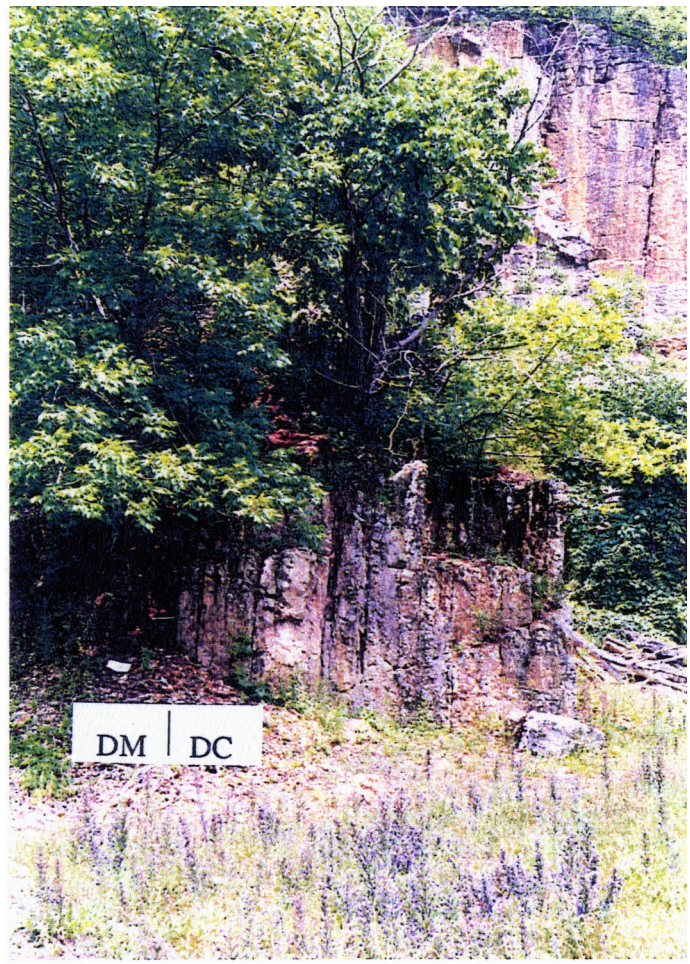

Figure 2.32. Photograph showing the Corriganville and the Mandata Formations from Monterey, VA (locality #17). The Field book sits on MTR-MD-3 and the contact between the Corriganville (DC) and the Mandata (DM) Formations is shown. The left side of the photograph is in a stratigraphically higher position.

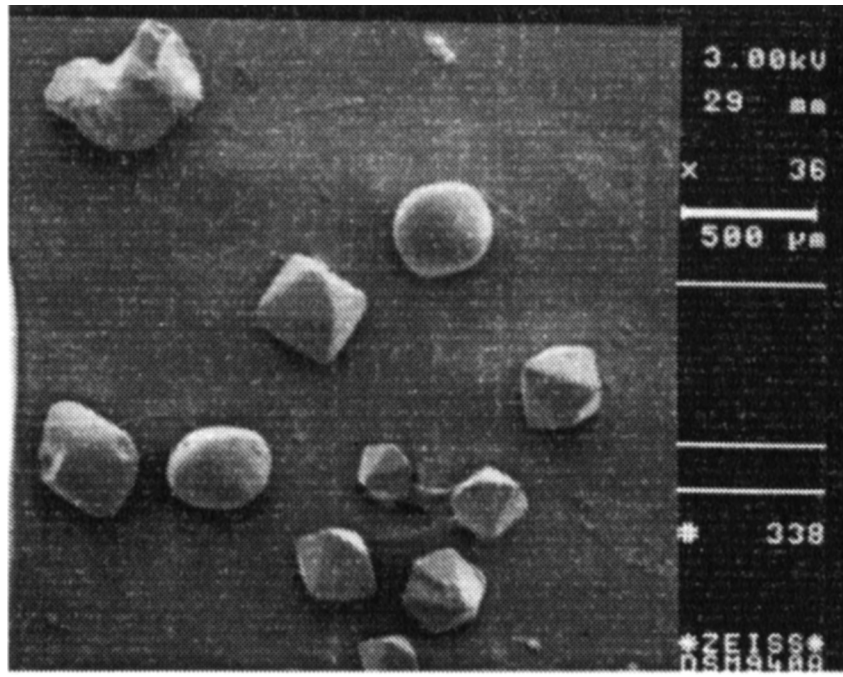

Figure 4.1. SEM photomicrograph of quartz crystals from CV-ES-11. The crystals from this bentonite display euhedral to rounded morphologies. All of these crystals contain melt inclusions. Note 500 µm scale bar on right side of image.

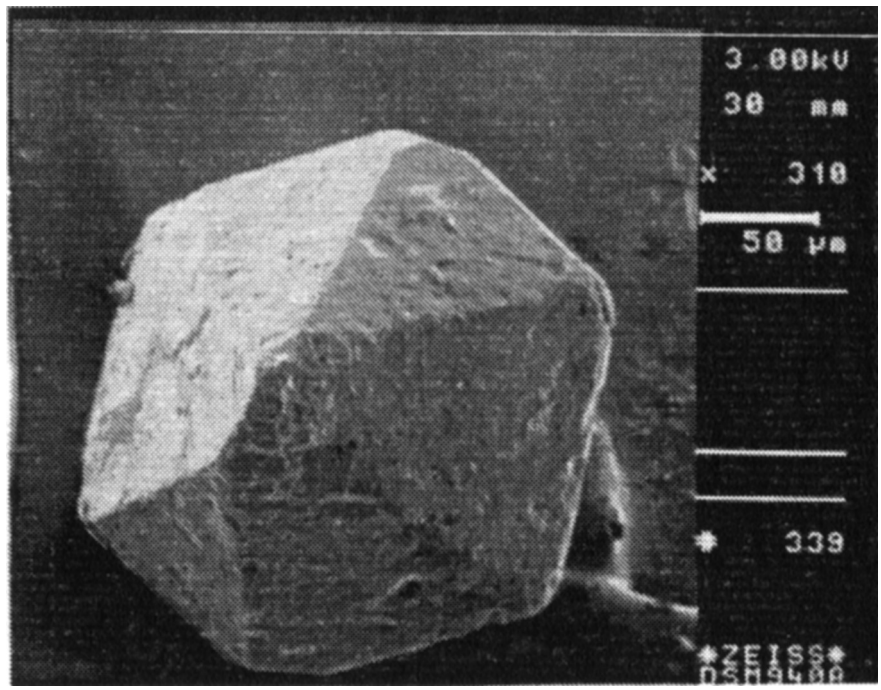

Figure 4.2. SEM photomicrograph of a quartz crystal from CV-ES-11. This crystal displays a well-developed euhedral morphology. Note 50 µm scale bar on right side of image.

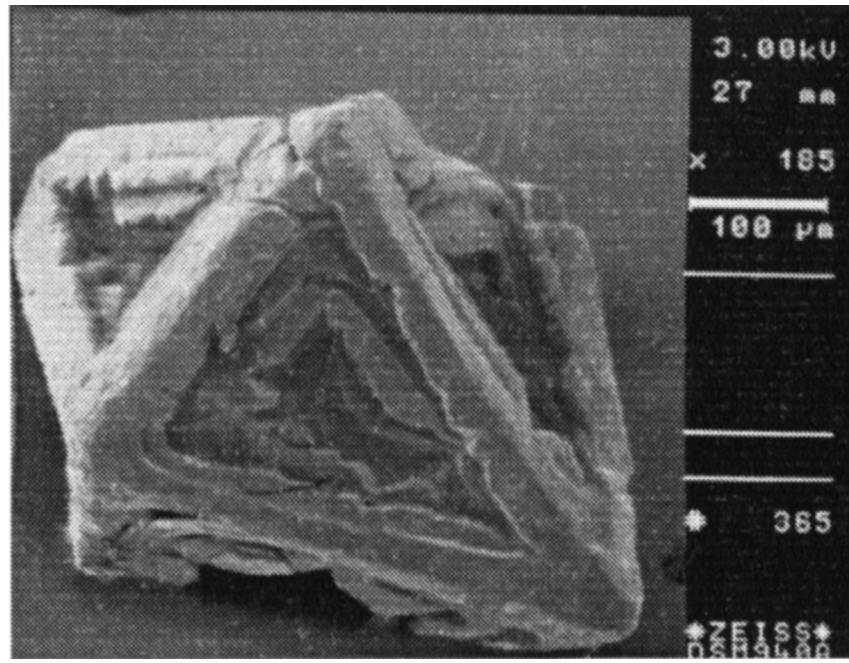

Figure 4.3. SEM photomicrograph of a quartz crystal from CV-ES-11 displaying triangular "hopper" reentrants on the crystal faces. The reentrants are stacked with reentrants that become smaller towards the center of the crystal. This crystal is broken parallel to the C-axis, which trends from the front right to the back left tips of the fragment. Note 100 µm scale bar on right side of image.

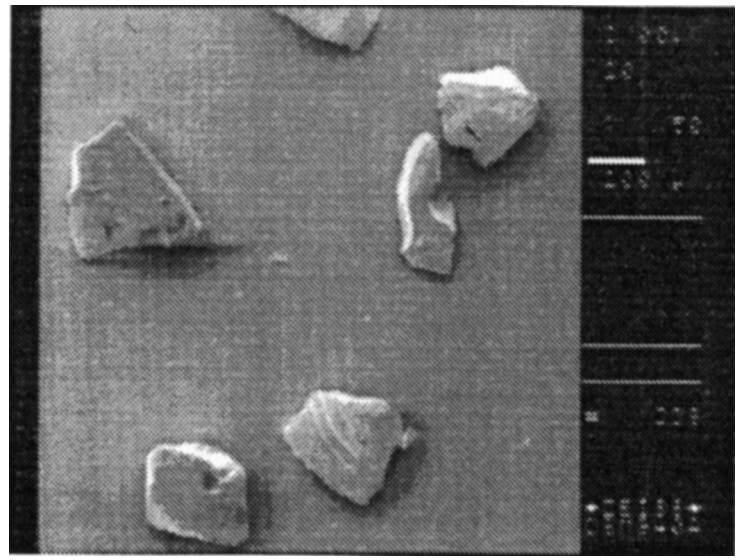

Figure 4.4. SEM photomicrograph of quartz splinters from BL-NS-8. Note the conchoidal fracture pattern on the surfaces of some of the crystals. The hollow voids on the surface of some of the splinters are thought to be spaces that were occupied by melt inclusions. Note 200 μm scale bar on right side of image.

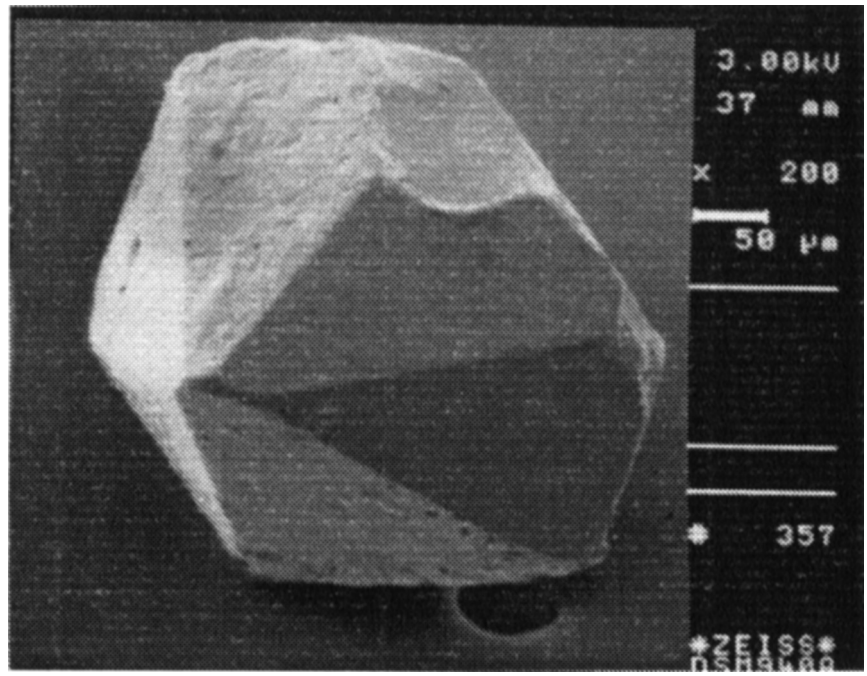

Figure 4.7. SEM photomicrograph of a beta-form quartz crystal from CV-ES-11. This crystal displays a reentrant at one of the A-crystallographic axes that is interpreted to be a yet unformed type 2 melt inclusion (see text). The C-axis of this crystal is horizontal. Note 50 µm scale bar on right side of image.

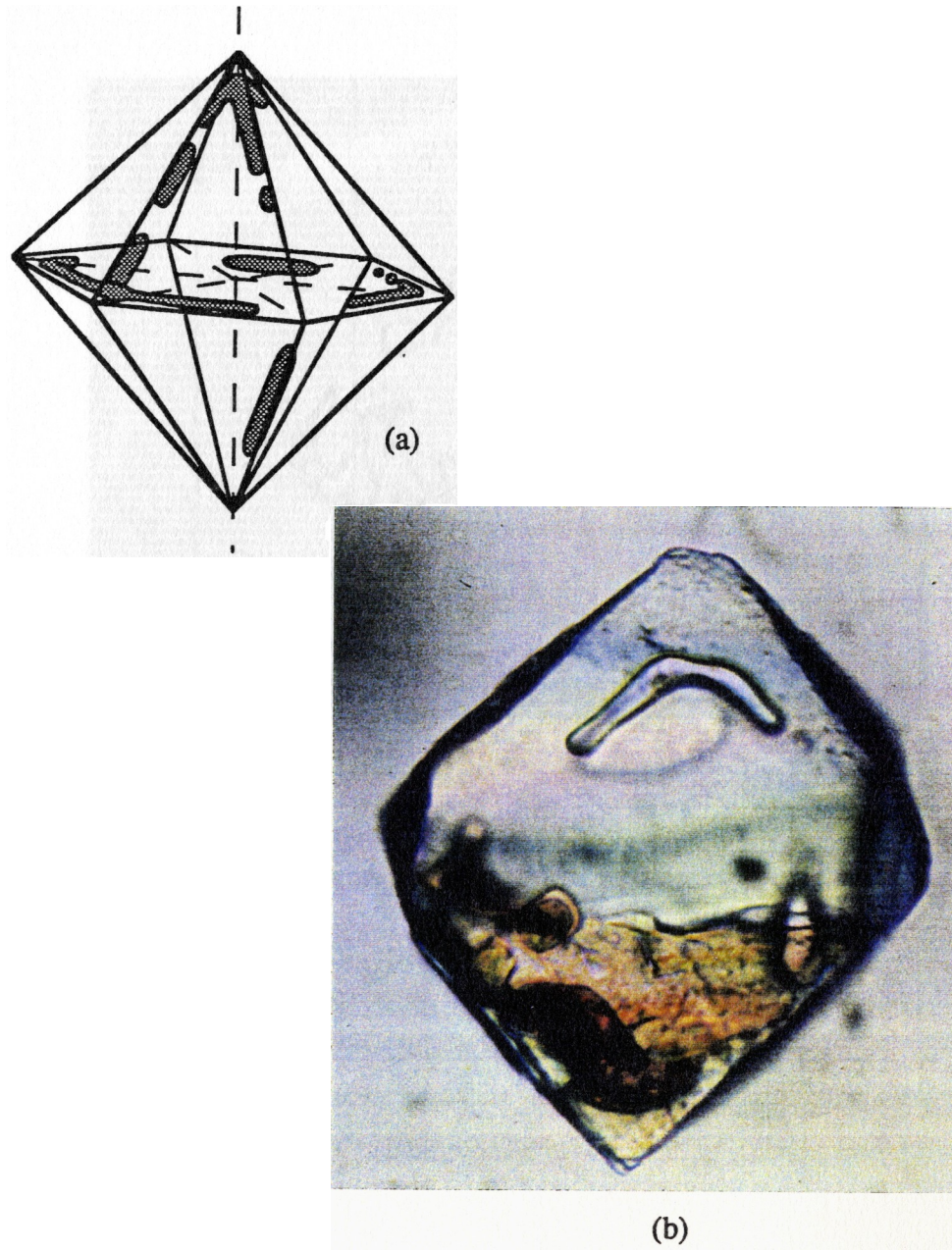

Figure 4.8. (a) Sketch of the outline of a beta quartz crystal containing type 3a and 3b inclusions. The C-axis of the crystal is vertical. These inclusions may be lobate or rounded and may join at corners to form elbow-shaped hybrid inclusions. (b) Photomicrograph of type 3 melt inclusions joined to form an elbow-shaped inclusion that mimics the shape of the crystal edges. The quartz phenocryst is from CV-ES-11 and is approximately 250 μm across.

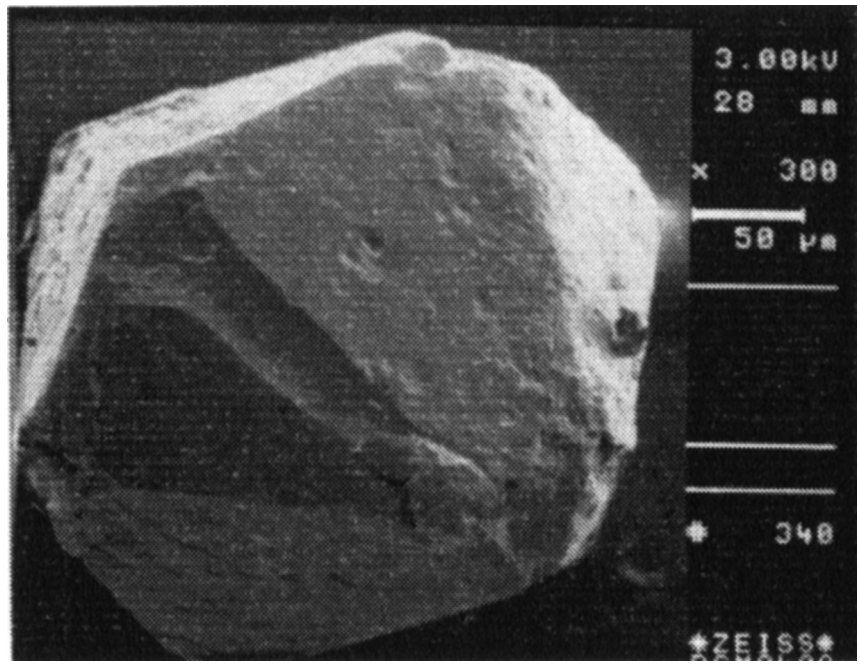

Figure 4.9. SEM photomicrograph of a beta-form quartz crystal from CV-ES-11. This crystal displays a long groove parallel to the intersection of the triangular crystal faces. This reentrant is interpreted to be a yet unclosed type 3 melt inclusion (see text). Note 50 µm scale bar on right side of image.

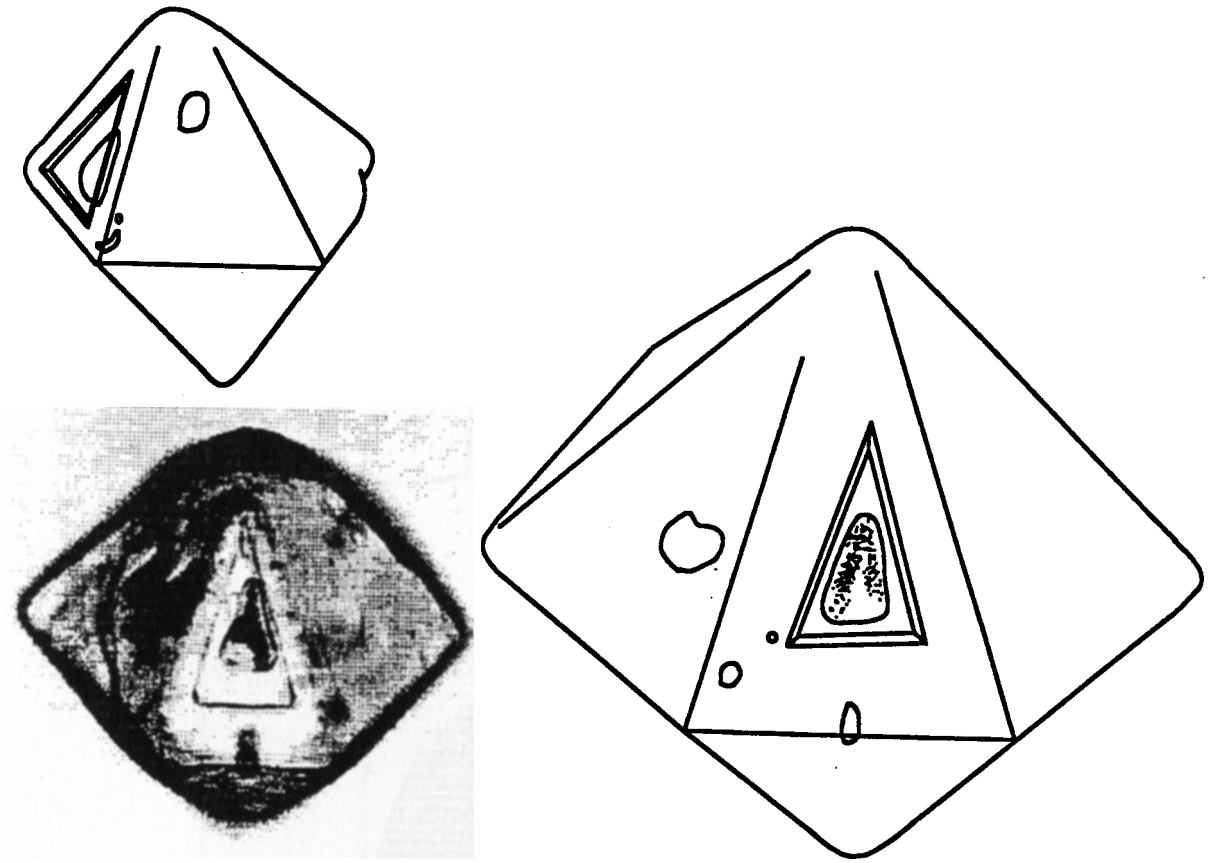

Figure 4.11. Transmitted light photomicrograph of a beta-form quartz crystal from CV-ES-11. This crystal contains a type 4 melt inclusion directly behind a triangular reentrant on the surface. The sketches show this crystal from different angles. The C-axis of this crystal is vertical and the crystal is approximately 275 μm in length.

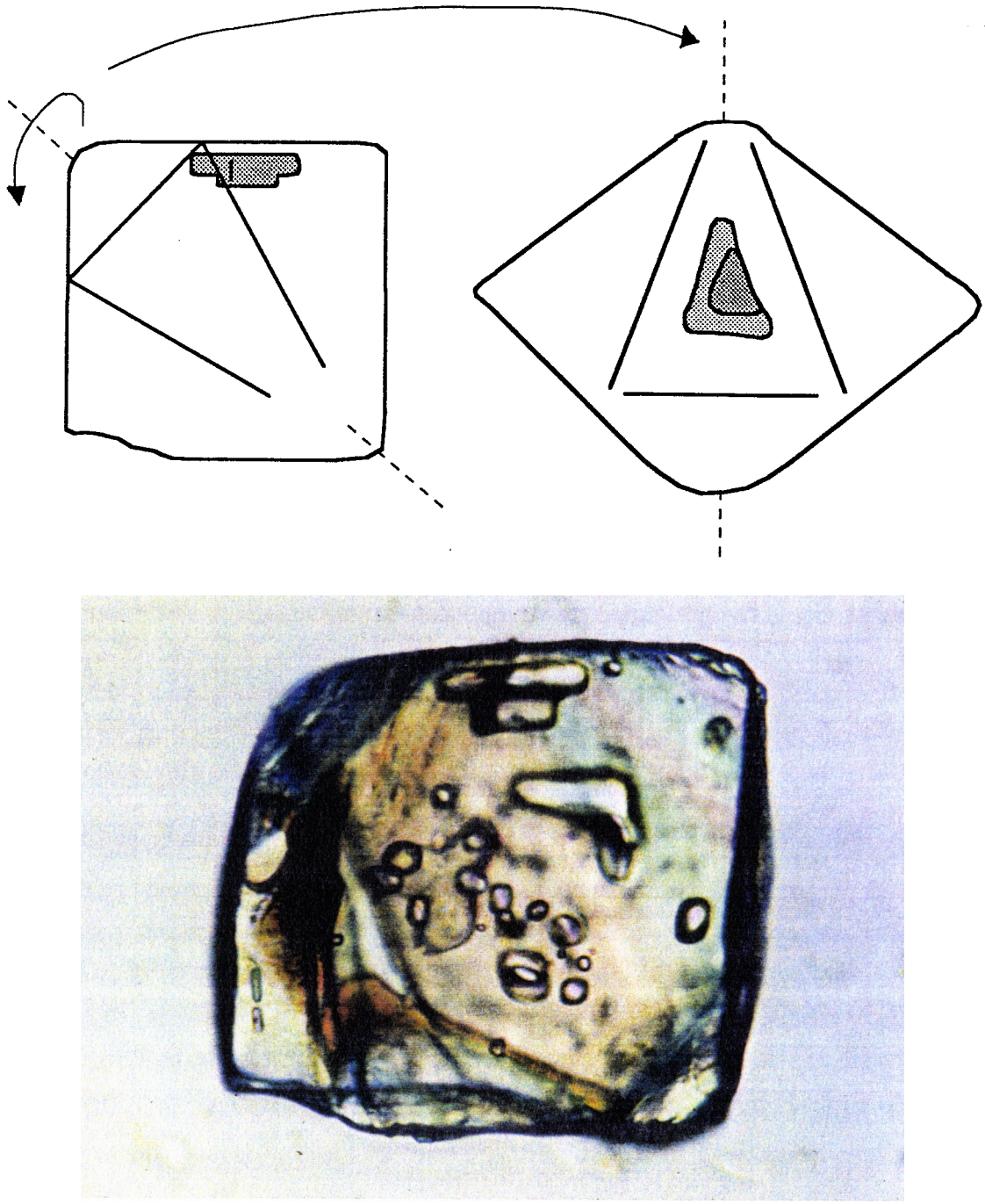

Figure 4.12. Transmitted light photomicrograph of a beta-form quartz crystal from CV-ES-11 displaying a two-level type 4 melt inclusion. The sketches show this crystal from two different angles. The right sketch shows the crystal rotated around the C-axis and tilted to the vertical in order to show the inclusion from two different angles. The crystal is approximately 275 μm in length.

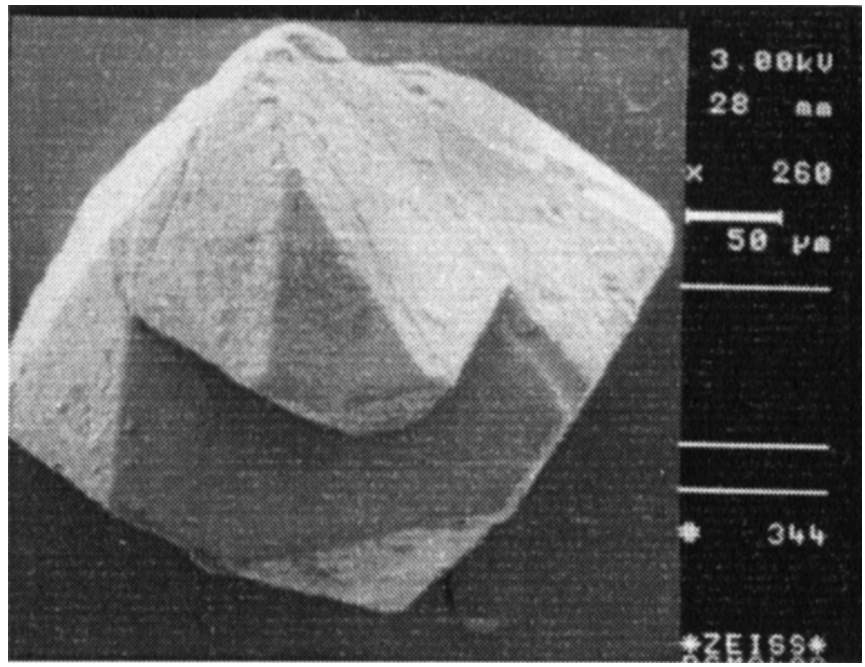

Figure 4.13. SEM photomicrograph of a quartz crystal from CV-ES-11. The crystal growth along one of the crystallographic axes appears to have been impeded for some time. Subsequent growth starting near the C-axis has produced a large segment of quartz extending from the top of the crystal, which, if growth had proceeded, may have entrapped a large inclusion similar to the one shown in Figure 4.14. Note 50 µm scale bar on right side of image.

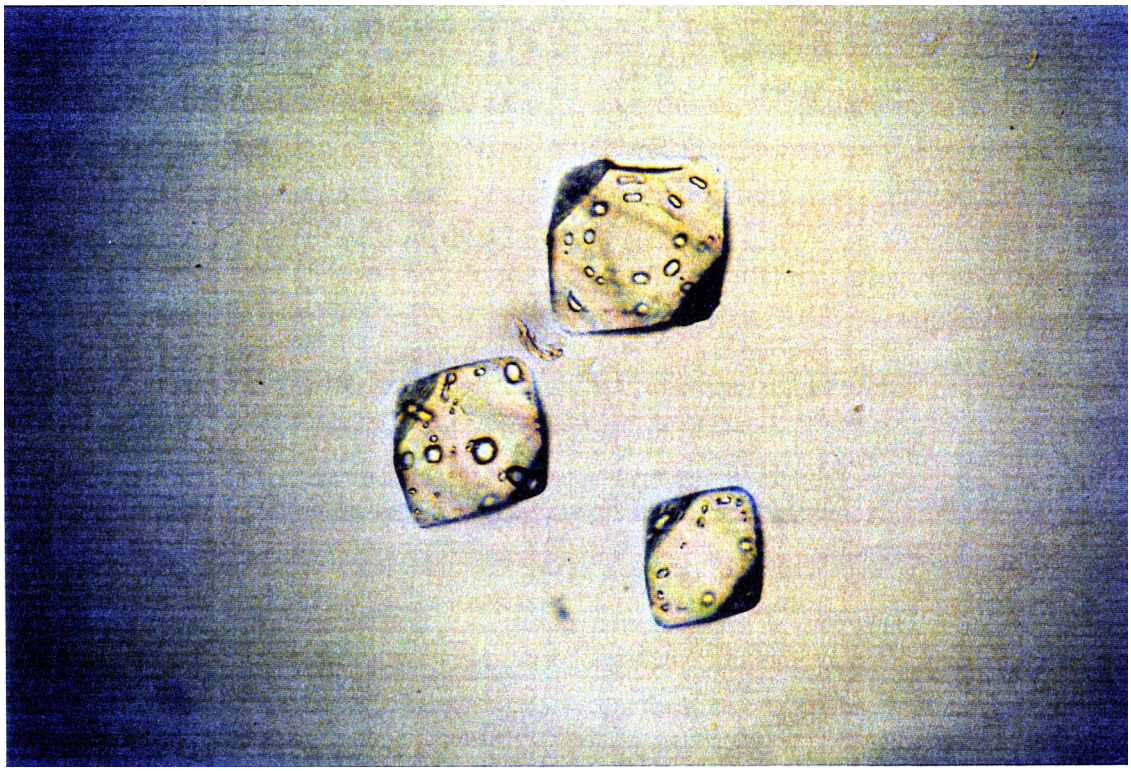

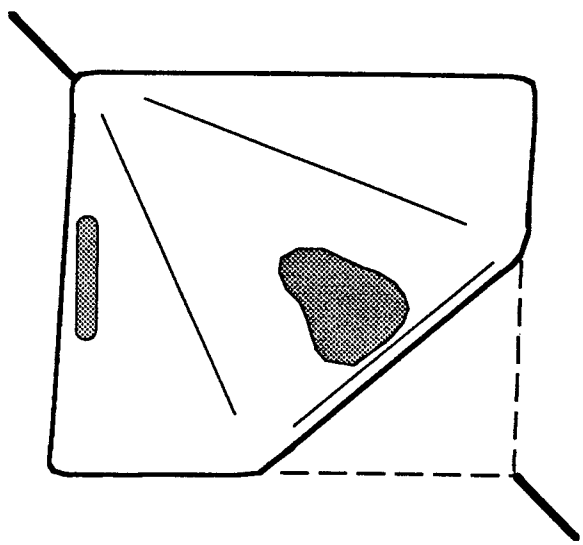

Figure 4.14. Transmitted light photomicrograph and a sketch of a quartz crystal from CV-ES-11. Crystal growth was impeded along the C-axis (thick line on sketch) and one of the A-axes. The dashed line shows the crystal outline if the crystal had grown normally.. The crystal is approximately 275 μm in length.

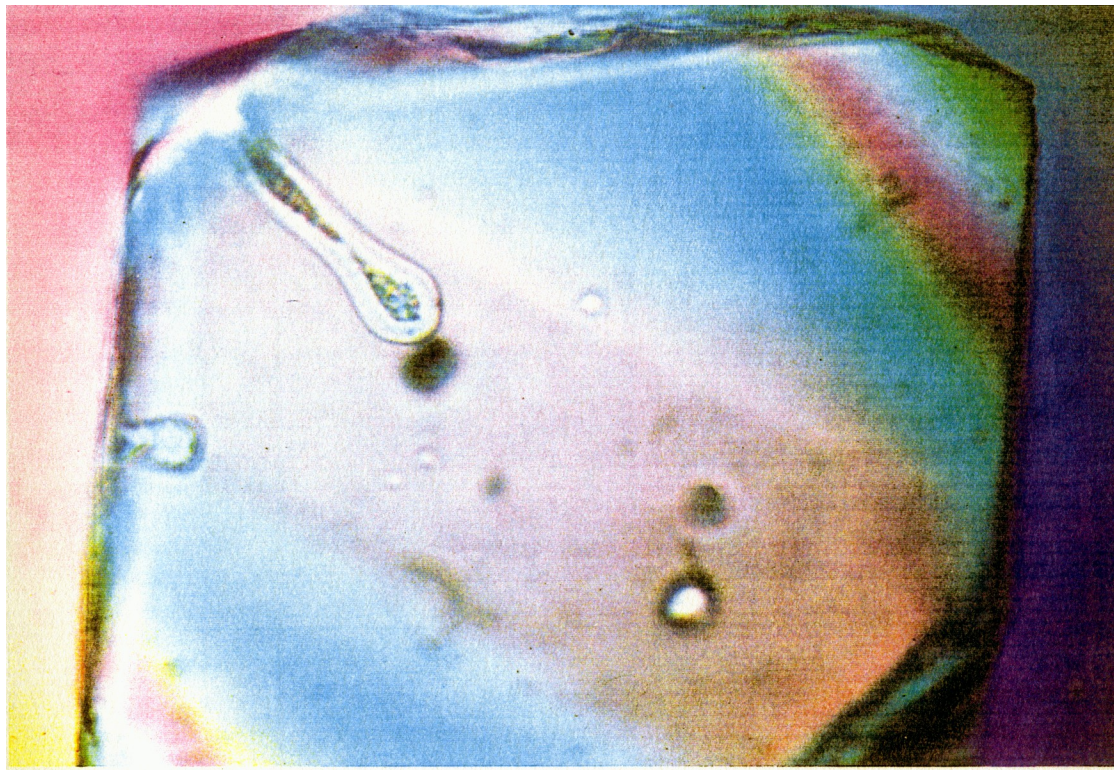

Figure 4.15. (c) Photomicrograph of a beta-form quartz phenocryst from CV-ES-11 showing two deep, narrow reentrants in the surface. These inclusions are texturally equivalent to the "hourglass" inclusions of Anderson et al. (1989). Field width of photo is 375 μm.

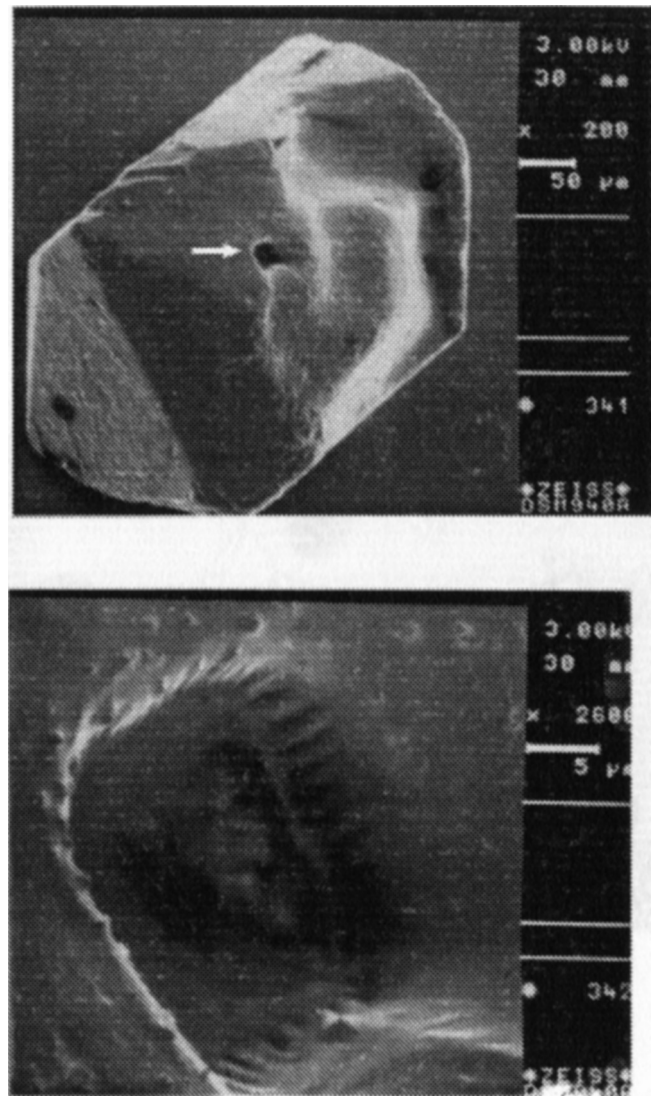

Figure 4.15. (a) SEM photomicrograph of a quartz crystal from CV-ES-11. The arrow points to a long, narrow reentrant in the crystal surface. (b) High-magnification image of the reentrant. Note the fine grooves at the end of the reentrant. This inclusion extends approximately 150 µm into the crystal. Note scale bars on right sides of images.

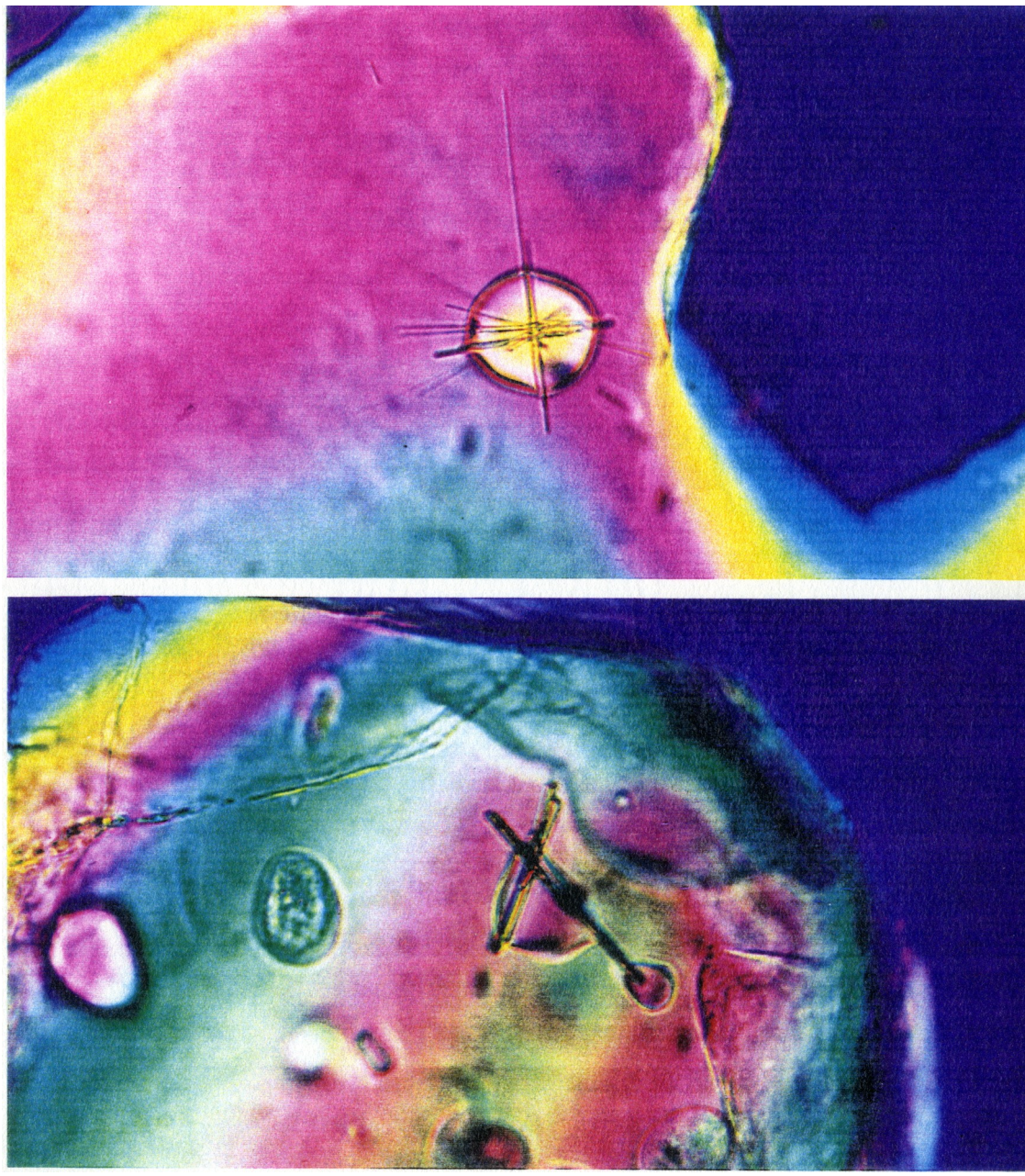

Figure 4.16. Photomicrographs of melt inclusions caused by impingement of the growing quartz crystal on another crystal causing melt to be entrapped in the quartz along with the crystal. Photomicrograph (a) is of a crystal from CV-ES-11 and the crystallite appears to be zircon. Photomicrograph (b) is of a crystal from the Ordovician Millbrig bentonite from Shakertown PA. This crystallite also appears to be zircon. Field width of photo is 375 μm.

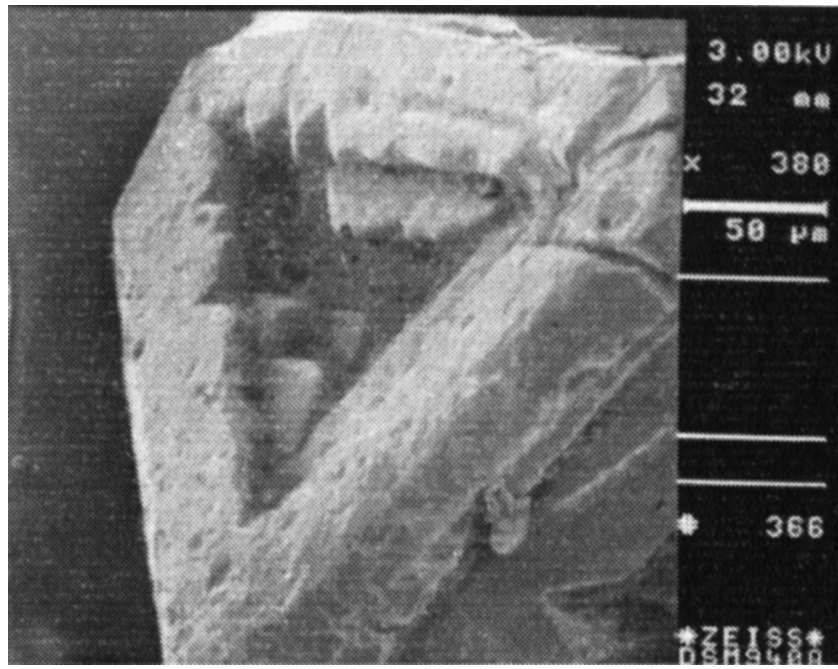

Figure 4.17. SEM photomicrograph of a skeletal reentrant on the face of a beta-form quartz crystal from CV-ES-11. This is an oblique view of the same crystal shown in Figure 4.3. The C-axis of the crystal is oriented from the lower right to the upper left of image. Note the triangular "teeth" growing from the edges of the reentrants towards the center of the crystal face. If these teeth would have continued growing they would have entrapped a type 4 melt inclusion. The growth of these teeth may be the result of a type of dendritic growth at high growth-rates in the presence of a significant boundary layer. Note 50 µm scale bar on right side of image.

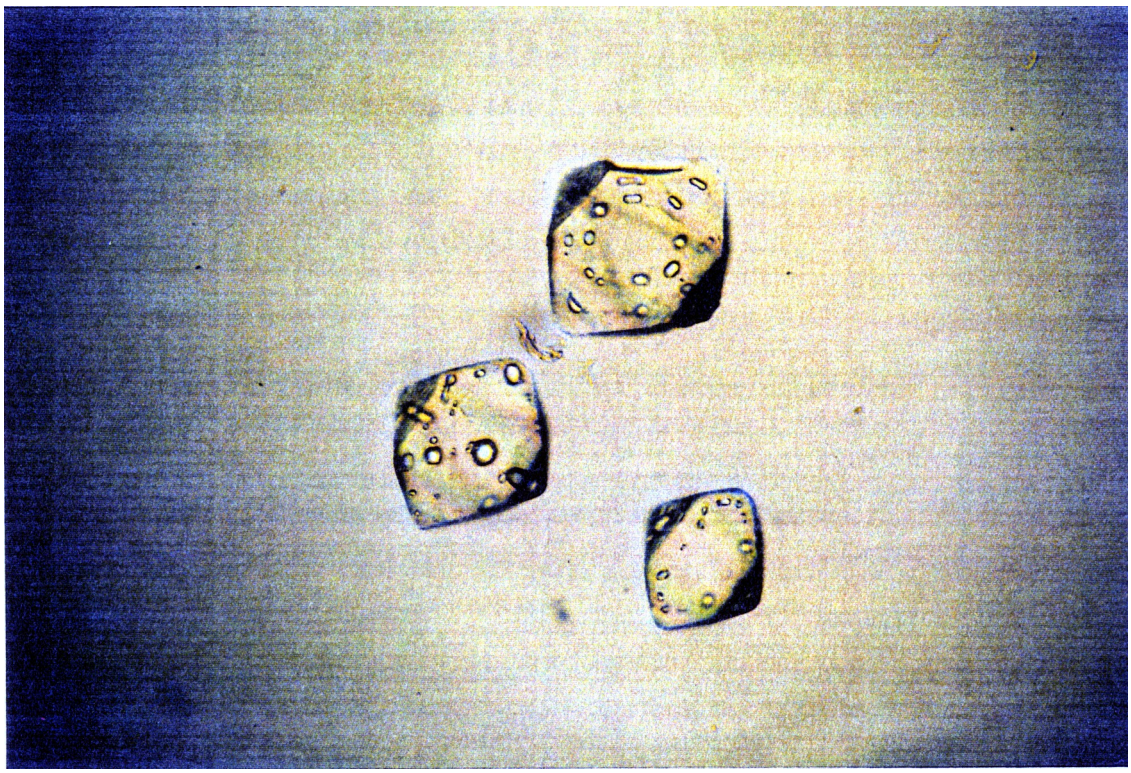

Figure 4.18. Photomicrograph of three beta-form quartz phenocrysts from CV-ES-11. These inclusions display "necklaces" of type 2 and 3b melt inclusions. All inclusions are the same distance from the edges of the hosts and the top crystal displays two layers arranged concentrically about the center of the crystal. Field width of photo is 500 μm.

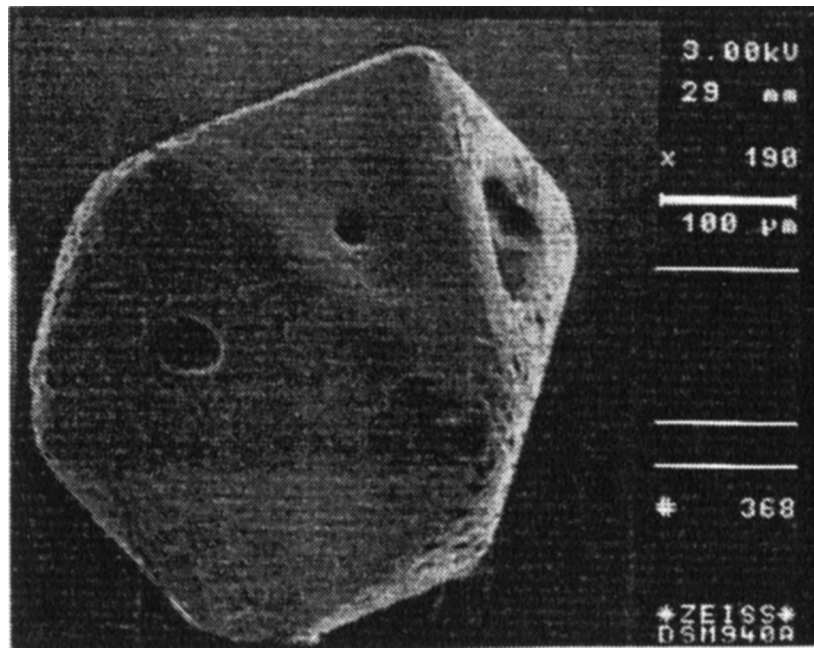

Figure 4.19. SEM photomicrograph of a rounded, beta-form quartz crystal from CV-ES-11. The crystal is rounded yet displays evidence of skeletal growth. Note 100 µm scale bar on right side of image.

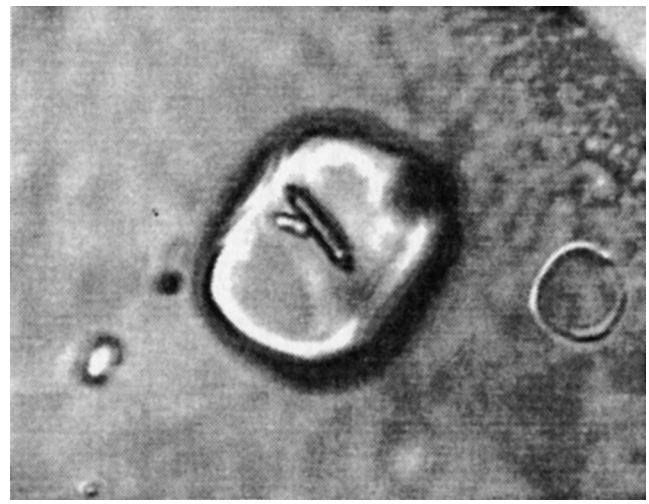

Figure 6.12. Photomicrograph of a zircon phenocryst within a melt inclusion in a quartz phenocryst from one of the Tioga bentonites from Frankstown, PA. Phenocrysts such as this clearly demonstrate that the melt is zircon-saturated and that the temperature of the melt can be inferred, if the Zr content is known, using the Zr systematics experimentally determined by Harrison and Watson (1983). Diameter of melt inclusion is approximately 50 μm.

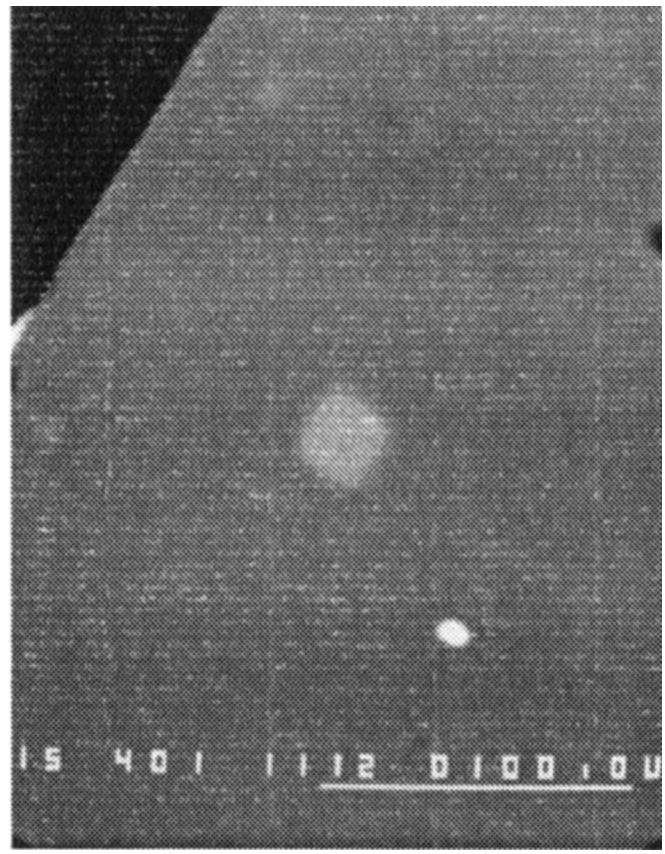

Figure 6.13. Backscattered electron micrograph of a monazite inclusion (bright inclusion) and a melt inclusion (gray, diamond-shaped inclusion) in a quartz phenocryst from CORR-MD-3. The presence of monazite inclusions and melt inclusions within the same quartz phenocrysts suggests that the melt was saturated with monazite and the systematics of LREE solubility in monazite-saturated melts can be used as a geothermometer. Note the 100 μm scale bar in the lower right corner. The black region at top left is epoxy.

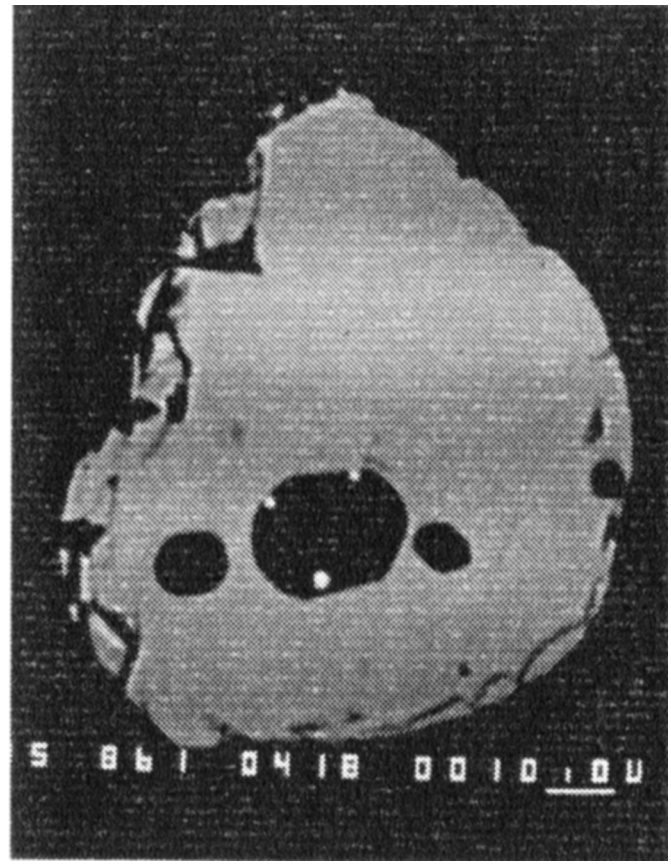

Figure 6. 14. Rhyolitic melt inclusions (three black spots) in an apatite phenocryst (surrounding gray region) from CAT-NS-1. The surrounding black region is the epoxy in which the specimen is mounted and the small bright spots are oxide inclusions within the melt inclusion. Note the 10 μm scale bar in the lower right corner.

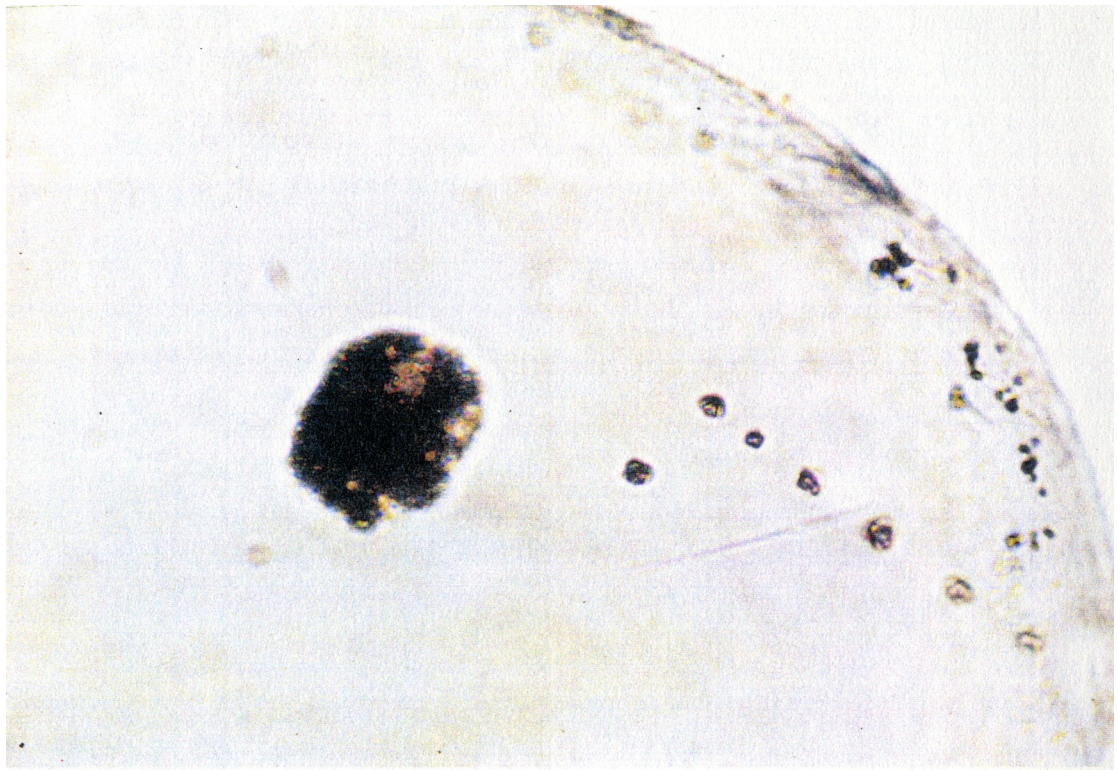

FIGURE 8.4a. Photomicrograph taken in plane polarized light of a crystallized melt inclusion in quartz from a Devonian bentonite from Limestoneville PA (Locality #10, LSV-MD-3). Note the irregular embayments in the inclusion walls. The prismatic inclusion is thought to be apatite. Width of field is 400 μm.

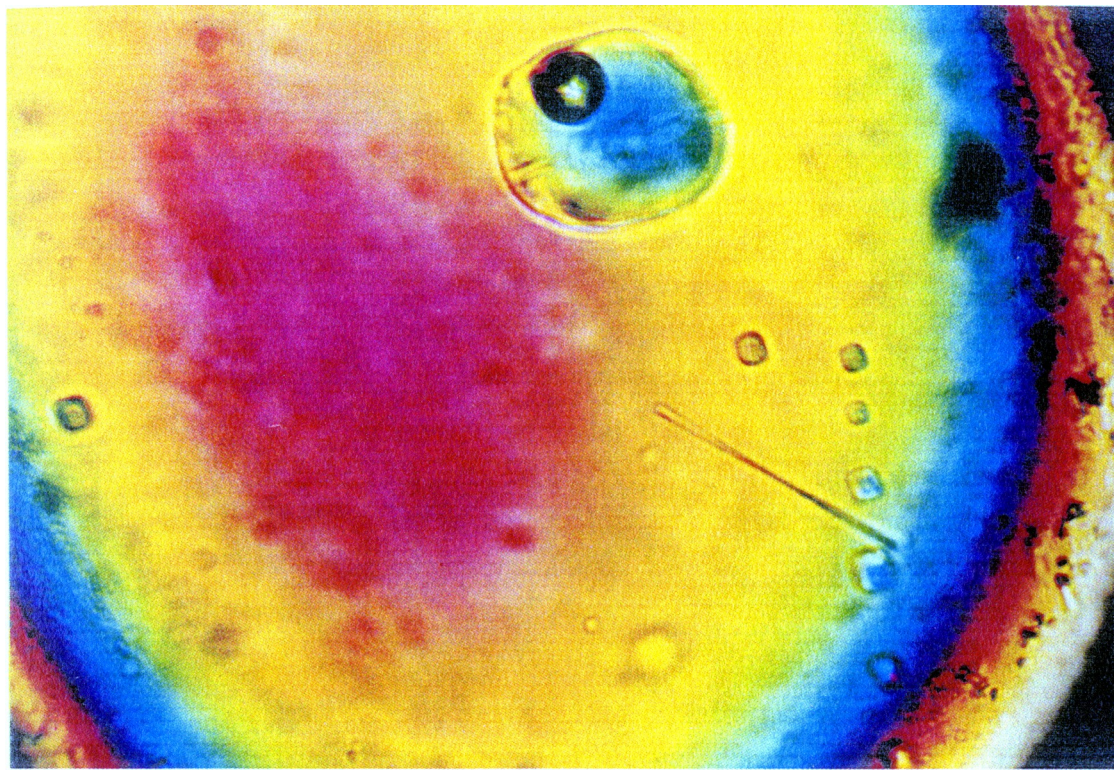

Figure 8.4b. Photomicrograph taken in polarized light of the same quartz crystal shown in figure 8.4a after it has been heated to 975° C. at 1 atmosphere in air for 168 hours. The inclusions are glassy and the large inclusion contains a vapor bubble. Width of field is 400 μm.

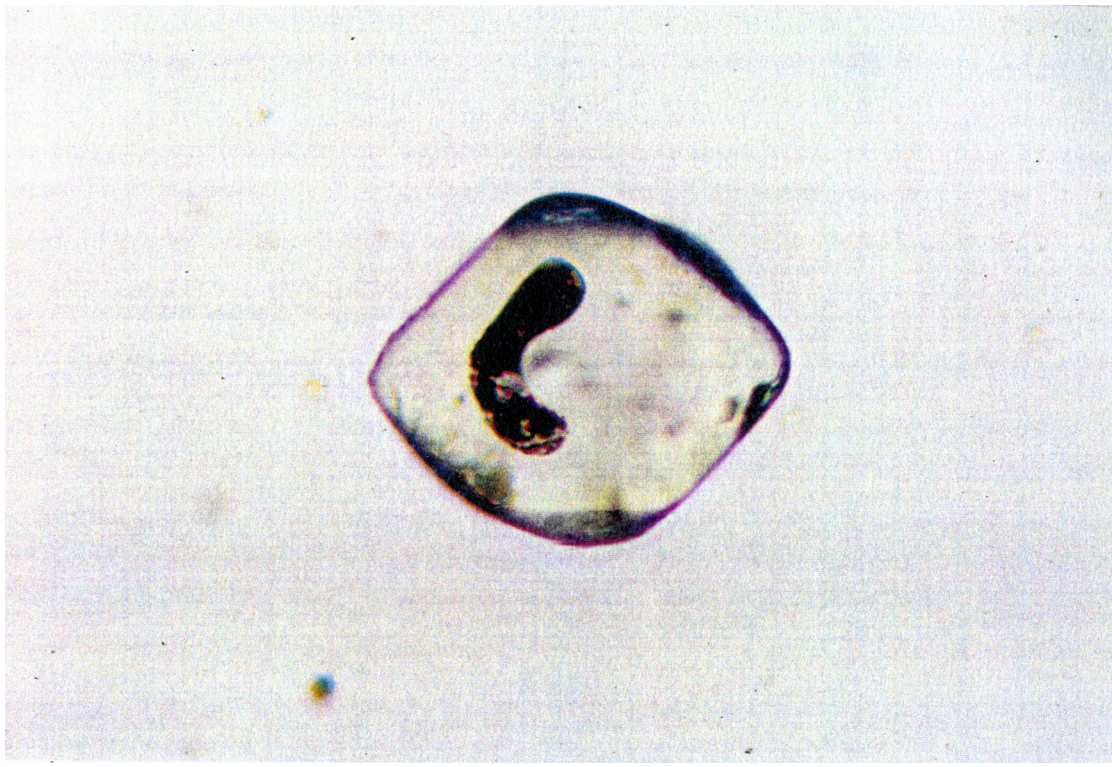

Figure 8.5a. Photomicrograph taken in plane polarized light of a lobate, crystallized inclusion in a rounded, beta-form quartz phenocryst from a Devonian bentonite from Limestoneville PA (LSV-MD-3). Width of field is 400 μm.

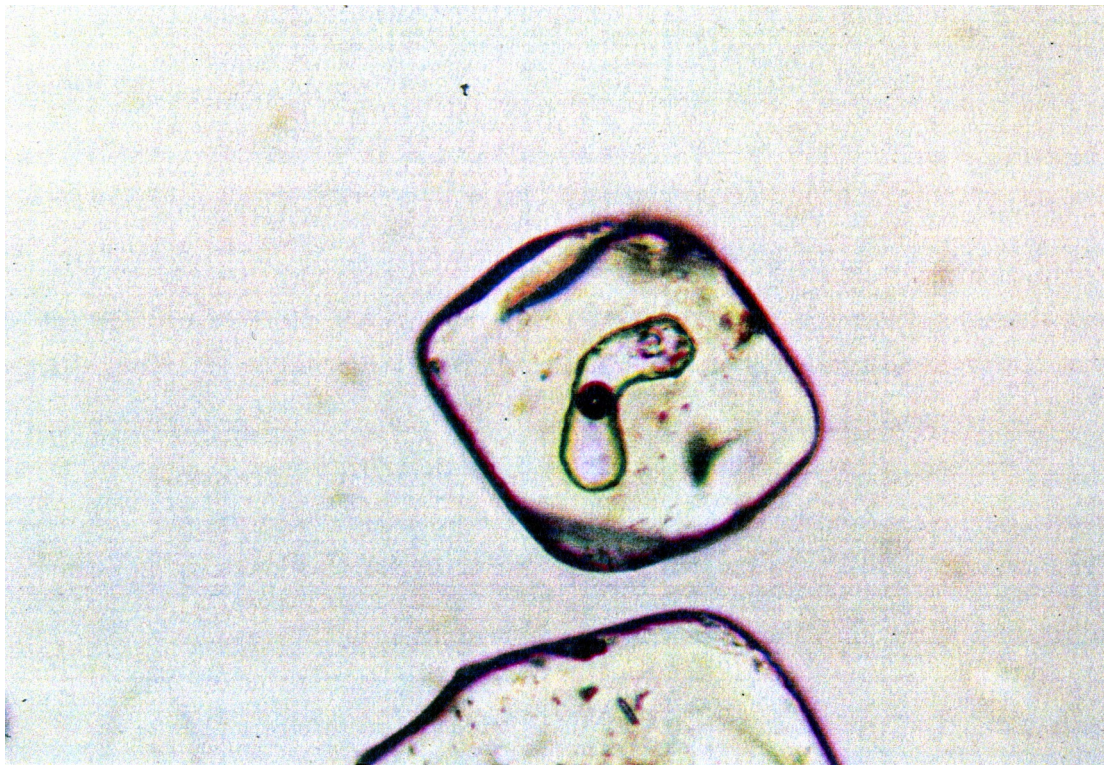

Figure 8.5b. Photomicrograph taken in plane polarized light of a euhedral beta-form phenocryst shown in Figure 8.5a after being heated to 975° C. at 1 atmosphere in air for 168 hours. The inclusion is glassy with a vapor bubble present. Width of field is 400 μm.

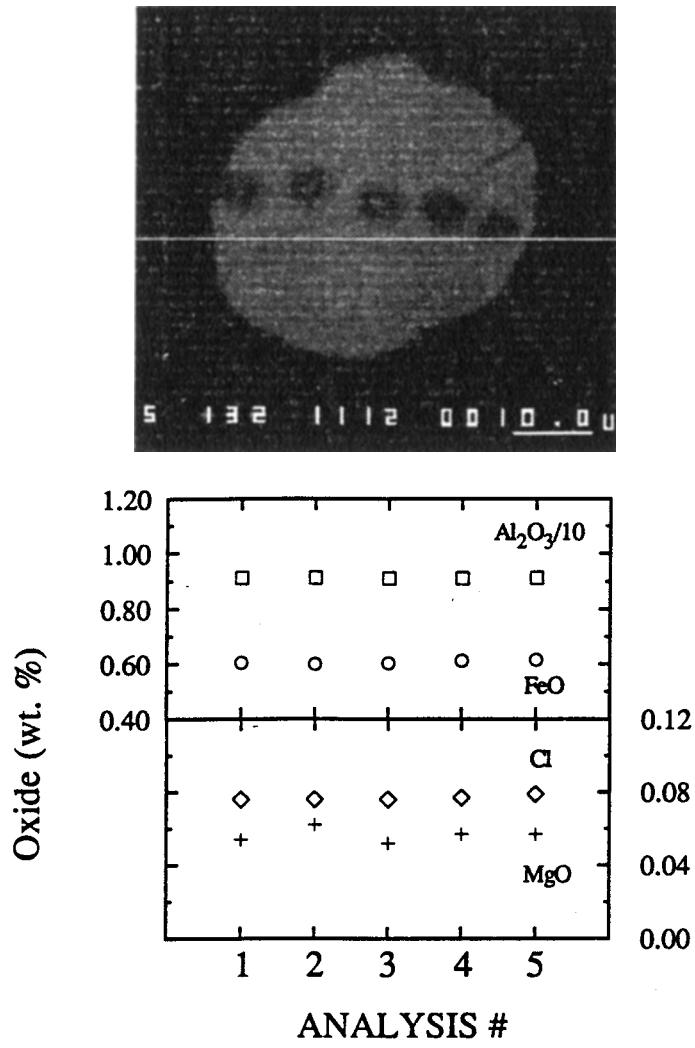

Figure 8.6. a) Backscattered electron image of the polished surface exposing the remelted inclusion in Figure 8.4. The black area is quartz host and the gray area is the melt inclusion. The round spots are the scars of electron microprobe analyses performed in order to test for chemical homogeneity of the glass. Figure 8.6b, c) The results of the analyses of the melt inclusion. The analysis number corresponds to the analysis scar above it on the micrograph. The glass is homogeneous within the analytical uncertainty of the analysis technique. Uncertainty based on counting statistics. Uncertainty associated with symbols with no error bars are less than the width of the symbol.

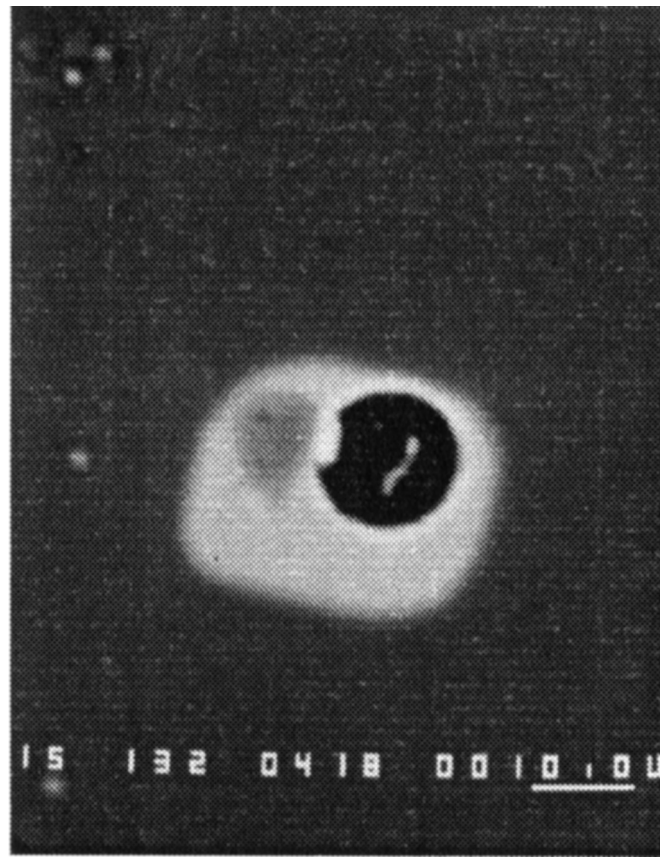

Figure 8.8. Backscattered electron image of a bubble in a small pristine inclusion from CAT-NS-1. The large light gray body is the melt inclusion with a scar from the electron microprobe beam (darker gray patch on left side of inclusion) and the black circle is the bubble. Scale bar in lower right is 10 μm.